Characteristics of waves guided by a grounded "left-handed" material slab of finite extent

J. Schelleng,[1] C. Monzon,[1] P. F. Loschialpo,[2] D. W. Forester,[2] and L. N. Medgyesi-Mitschang[2]
[1]*SFA/NRL, Largo, Maryland 20774, USA*
[2]*Naval Research Laboratory, Washington, D.C. 20375, USA*
(Received 29 September 2003; revised manuscript received 13 July 2004; published 6 December 2004)

The properties of waves guided by a plane-parallel finite slab of material having an ideal, homogeneous, and causal permittivity $\varepsilon(f)$, and permeability $\mu(f)$, are investigated analytically and numerically through simulations done via a finite difference time domain (FDTD) code. Lorentzian functional forms are chosen for $\varepsilon(f)$ and $\mu(f)$. Wave guidance is examined for frequency ranges where the material in the slab is in the left-handed material (LHM) regime, i.e., the real parts of $\varepsilon(f)$ and $\mu(f)$ are negative. It is shown that for reasonably thin slabs, and unlike ordinary materials, there is a unique power recirculation or feedback mechanism wherein the fields in the vicinity of the slab exchange power across the free-space/LHM slab interface. Within the LHM slab, the power travels backwards towards the source. This results in significant but bounded energy accumulation near the edge of the slab closest to the source. The energy exchange across the slab interface is necessary in order to sustain the resulting backward wave in the slab. Slabs thicker than a wavelength are also analyzed, leading to a reversal of the power loop description. The agreement between analytical and numerical results is excellent. They confirm the guided wave physics of a LHM slab.

DOI: 10.1103/PhysRevE.70.066606 PACS number(s): 41.20.Jb, 42.15.Dp, 42.25.Fx, 42.25.Bs

I. INTRODUCTION

It is a well-established fact that for simple geometries, electromagnetic power travels away from the source. In the course of numerical simulations, we became aware that there are some conditions under which power recirculation backwards towards the source exists in a grounded left-handed material (LHM[1]) slab.

Guided waves in penetrable layers have been studied extensively for "ordinary" materials where $\mathrm{Re}[\varepsilon(f)]>0$ and $\mathrm{Re}[\mu(f)]>0$. Two major types of guided waves can be distinguished: the forward waves and the backward waves [1,2]. An example of the former is the familiar end-fire radiation of finite radiating structures. Backward waves are more complex. They radiate in the direction of the source and thus can contribute significantly to backscattering. Backward waves are very difficult to produce using homogeneous material layers. To the authors' knowledge, the existence of backward waves in a *homogeneous* layer requires the intrinsic properties of a material layer to be anisotropic and nonreciprocal, such as a biased ferrite or a moving medium. No homogeneous isotropic medium is known to be capable of sustaining backward wave operation in the grounded slab configuration. However, as shown here, a grounded homogeneous LHM slab, where the conducting surface is an integral part of the structure, does produce a power recirculation at the slab interface that depends on a dominant backward wave within the slab itself.

Veselago introduced the concept of a LHM as a *Gedanken* experiment 35 years ago [3]. As noted above, such a material is characterized by simultaneous negative $\mathrm{Re}[\varepsilon(f)]$ and $\mathrm{Re}[\mu(f)]$. These materials have the rather unusual property that the phase velocity and the energy flow are in opposite directions [4–11].

Materials used to date for experimental replication of LHM properties have been composed of discrete elements smaller than the wavelength of illumination [8–12]. The materials typically consist of periodic arrays of wires and split ring resonators (SRR). The latter were first proposed by Pendry [13]. Left-handed behavior is then observed in selected frequency regimes. Previously we have demonstrated that the periodicity in these LHM syntheses produces multiple reflection and transmission bands analogous to those observed with photonic band-gap materials and frequency selective surfaces (FSS) [12].

Shadrivov *et al.* in a recent paper dealt with guided modes (eigenmodes) in an infinite LHM slab [14]. Unlike the finite grounded LHM slab considered here, the infinite slab in [14] is in free space (ungrounded) and lossless, i.e., the material is noncausal. The polarization is orthogonal to the present one.

II. ANALYSIS

Our investigation was carried out both numerically and analytically. The numerical simulations were done via an FDTD code [15,16], requiring causal material parameters. A parallel theoretical analysis for a grounded infinite homogeneous LHM slab was used to provide additional insights into the physics of the problem. These results supported the principal conclusions from the FDTD simulations.

A. FDTD simulations

For physically meaningful electromagnetic propagation in any medium, it is important that the constitutive parameters be causal. Previously Lorentzian, Debye, and Drude models

[1]Here "left-handed" is not associated with handedness but with negative refraction. We follow the terminology introduced by Veselago that is widely accepted at the present time. Alternately, such materials are also designated in the literature as negative index materials (NIM).

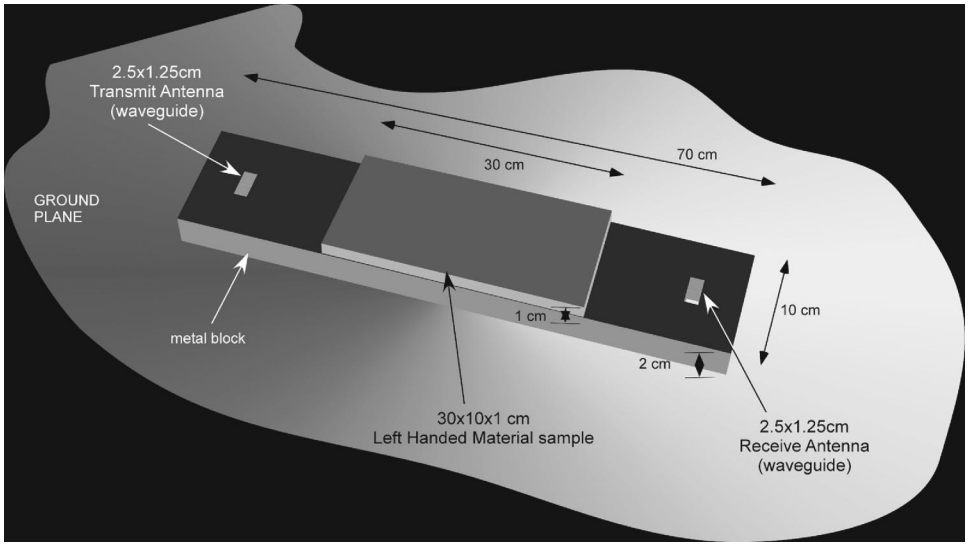

FIG. 1. Geometry of the FDTD model involving a grounded 1-em-thick LHM slab.

have been employed in connection with LHM media. It is known that to obtain negative (real) index of refraction properties over a limited frequency range, both the intrinsic permeability $\mu(f)$ and the permittivity $\varepsilon(f)$ must be strongly dispersive. In the present study, we have adopted a Lorentzian frequency-dependent medium for both $\varepsilon(f)$ and $\mu(f)$. It is of the form

$$F(f) = 1 + \frac{K-1}{1 + j\left(\frac{fG}{f_o^2}\right) - \left(\frac{f}{f_o}\right)^2}. \quad (1)$$

We focused on materials where $F(f)=\varepsilon(f)=\mu(f)$. This choice minimizes impedance mismatches avoiding multiple reflections that can obscure the wave propagation features within the slab. The resulting medium has a complex index of refraction $n(f)$ with $\mathrm{Re}[n(f)]$ acquiring positive, negative, or zero values as the frequency is varied. This allowed us to investigate the physics of propagation over a broad spectrum. In the simulations $F(f)=\mu(f)$ or $\varepsilon(f)$ and $K=\mu_{\mathrm{DC}}$ or $\varepsilon_{\mathrm{DC}}$. To reduce the effect of losses, in Eq. (1) we selected $G=0.04$ GHz, $\varepsilon_{\mathrm{DC}}=\mu_{\mathrm{DC}}=4.0$, and $f_o=6.3$ GHz. The calculations were carried out around $f=10$ GHz, where the Lorentzian index takes on a value of $n=-1.001-j0.013$.

The specifics of the three-dimensional (3D) geometry used in the simulations is given in Fig. 1. The LHM sample is 30 cm long by 10 cm wide and 1 cm thick (i.e., a slab is one-third of a wavelength). It rests on a 70-cm-long metal block. Open-ended waveguides embedded in the metal block are used as transmit and receive antennas, terminated with 50 Ω coax lines. The whole fixture rests on a ground plane. In the simulations, we initially excited the transmit antenna with a 10 GHz CW pulse at $t=0$ with a duration 3.2 ns.[2]

The FDTD code for the simulations has been validated extensively by laboratory experiments [15,16]. The code uses PML (perfect matching layer) absorbing boundaries in the dimensions of finite extent. A perfect magnetic conductor is used to realize a symmetry plane through the center of the sample [17]. A time step interval of 1.9 ps (Courant condition) was used in all computer runs.

Figure 2 depicts FDTD "snapshots" of the electric fields (a) during the CW pulse and (b) after the CW pulse. There are four components of these fields. They are (1) P_1 is the incident wave propagating on the ground plane from the source, (2) P_2 is the wave that has penetrated into the slab, (3) P_3 is the surface wave along the free-space/LHM slab interface, and (4) P_4 is the backward wave within the slab itself. Note there is no phase reversal along the top of the slab. Hence the phase fronts of the transmitted field in the slab must travel away from the source. On the other hand, according to Veselago [3], we know that phase and power travel in opposite directions in a LHM medium. Specifically, the power P_4 in the LHM slab travels backwards towards the source, resulting in a finite but significant energy accumulation at the slab edge closest to the source. This is the reverse of the effect encountered for a LHM slab for normal incidence [3]. In that case, the power in the slab travels away from the source while the phase travels towards the source.

Figure 2 also shows that a high-field concentration in the leading-edge region exists. Any discontinuity that interrupts the backward power flow in the slab leads to a region of high energy density. Additional FDTD simulations, not shown here, reveal that the field oscillations persist $t>9$ ns due to the high Q of the material (low loss), and that the radiation occurs principally at the edges of the slab. Note, the curvature discontinuities (kinks) in the phase fronts at the free-space/LHM interface on top of the slab are clear evidence of power recirculation between the free-space region and the LHM slab, i.e., P_3 and P_4 are in the positive and negative x direction, respectively.

In the following simulations, we excited the transmit antenna with a 10 GHz CW pulse at $t=0$ with a duration sufficiently large to verify that the time-harmonic state was reached. Figure 3 presents a snapshot of the electric fields at $t=50$ ns after the start of the CW pulse (i.e., after about 500 periods), together with the Poynting vector calculations

[2]While the fields at the receive antenna were also calculated, their discussion is omitted since they play no role in the power recirculation mechanism.

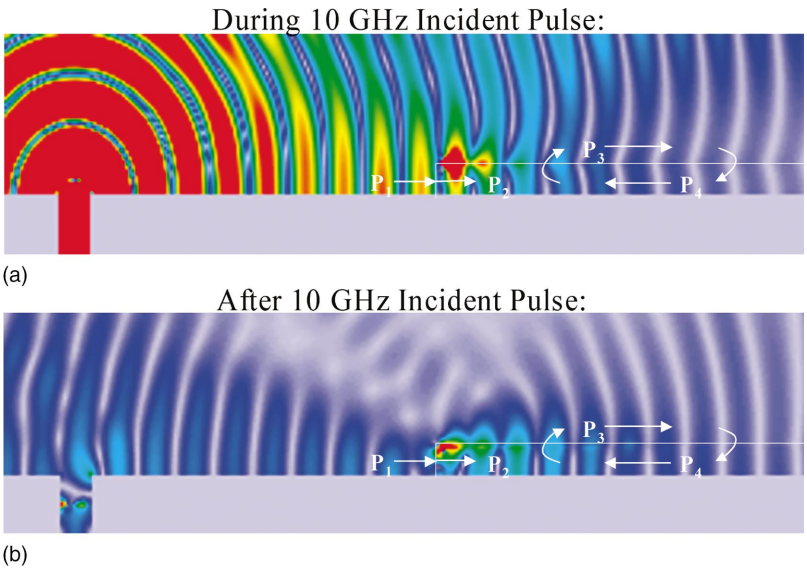

FIG. 2. (Color) FDTD "snapshots" of the electric fields during (a) and after (b) the CW pulse. The figure illustrates that remarkably, power recirculation exists at the top surface of the slab, due to the fact that power within the LHM slab travels backwards towards the source. The power circulation between air and slab is evident from the phase front discontinuities (kinks). The figure also illustrates the high field concentrations near the leading edge. Cases (a) and (b) correspond to $t=2.86$ ns and $t=4.25$ ns, respectively. At 10 GHz the slab is one-third of a wavelength thick.

along a plane bisecting the slab. The two lower figures in Fig. 3 depict the x-directed Poynting vector P_x in the vicinity outside and inside of the leading edge of the slab. Inside the slab $P_x<0$, i.e., directed in the negative x direction, confirming that the fields in the LHM slab are principally backward waves. The small positive ripples for P_x occurring for $t>3$ ns are consistent with the presence of reflected rays. This is due to the fact that the initial pulse from the source reaches the leading edge of the slab at $t\sim 1$ ns, and it takes the pulse ~ 2 ns to make a complete traversal back to the leading edge. Outside the slab P_x is predominantly positive, except for the contributions of the fields reflected from the leading edge beginning at $t\sim 1$ ns.

Further examination of the FDTD results reveals that for early times, when the wave packet first hits the leading edge, the phase fronts in the slab are reversed, indicating negative refraction. In other words, during the early times the energy transmission into the slab takes place initially through the edge and not through the top surface of the slab. Thus the power in the LHM slab travels initially away from the leading edge, while the phase front travels towards the leading edge. This was previously demonstrated for a slab at normal incidence [16]. As the incident wave progresses along the free-space/LHM interface, evanescent fields become predominant. This was confirmed from the theoretical analysis. The dominant mode inside the slab must carry power towards the leading edge, but initially it is minimum. As time passes, power begins to leak into the slab, and the power flow to source occurs through the backward wave mode over the entire length inside the slab.

The FDTD computations of the time-varying Poynting vector field distribution for the finite slab were carried out for time t sufficiently large so as to ensure that the time-harmonic (steady-state) regime was reached. It was found, however, that the time-harmonic field snapshots (after several hundred periods) are essentially identical to those obtained after 30 periods. For brevity, in the presentation no similar snapshot will be presented in this context. The results

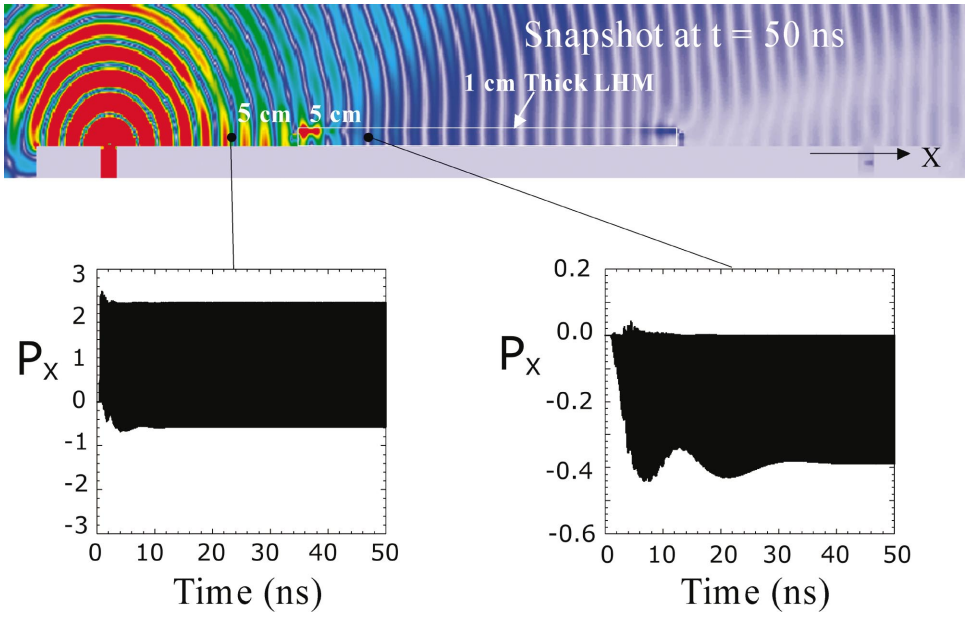

FIG. 3. (Color) Poynting vector along the slab (central plane cut). The top figure is a snapshot at 50 ns after the start of the CW pulse. The lower figures depict the x-directed Poynting vector outside (left) and inside (right) of the leading edge of the slab. The convergence of the Poynting vector magnitude is a clear indication that the time-harmonic regime has been reached.

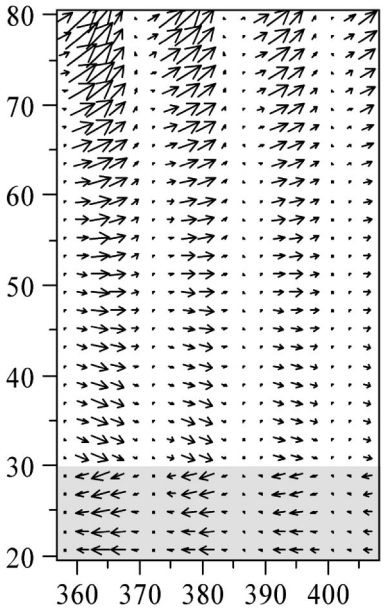

FIG. 4. FDTD time-harmonic $f=10$ GHz Poynting vector field in the neighborhood of a LHM slab, calculated after 500 periods. The vector field is mapped for 356 mm$\leqslant x \leqslant$408 mm. The LHM slab is the region 20 mm$\leqslant z \leqslant$30 mm. The magnitude and direction of the arrows correspond to the local Poynting vector. Although the power in the slab flows eminently towards the source (left), the power above the slab points away from the slab (right), and can be significantly larger, resulting in a net power flowing away from the source. The FDTD simulation consisted of 1000 periods.

are presented in Fig. 4 in the form of Poynting vector fields, corresponding to 50 ns (500 periods) for a slab with thickness $h=1$ cm at $f=10$ GHz, where $\varepsilon=\mu=-1.001-j0.013$. In Fig. 4, the z component of the Poynting vector field is magnified fivefold to show the power flow in more detail. The figure shows that power is drawn from the incident field along the whole length outside the top of the slab to feed the layer-bound backward wave inside the slab.

Other calculations not shown here confirm that as the losses increase, the power feedback becomes more pronounced, with the Poynting vector field tilting even more, demonstrating that more energy couples from the evanescent fields in the free-space region into the backward wave within the slab. Also, other calculations not shown corresponding to earlier times (about 30 periods) do contain a very small upward pointing component for the Poynting vector inside of the slab. These are the effect of transient fields due to higher-order modes in the slab, and they do die out for larger times.

We have carried out further studies of the phase front behavior at later times not shown here. They confirm that once the incident wave packet has subsided, remnants of a reflected wave packet as well as interference between backward waves inside the slab are operative. The internal fields do persist over a long period of time, indicating that the LHM slab is a high Q structure. This is consistent with the choice of parameters in Eq. (1), picked earlier to ensure low loss.

We have also studied the effect of the thickness parameter, and found that as the thickness increases and exceeds the free-space wavelength, a combination of higher-order modes resembling Veselago's lens fields (i.e., power normal to the slab front edge is continuous) will become dominant inside the slab, inverting the state of affairs, i.e., the power inside the slab will be directed away from the source, while the power right above the slab will flow towards the source. We observe that well above the slab boundary, power is directed away from the source (this is as expected, so that the net power flow is away from the source). Figure 5 helps illustrate this by comparing the fields in the 1 cm case with those in a 5 cm slab configuration. Figure 5(b) shows explicitly polaritons and higher-order modes which peak at the metal interface and appear to be related to direct transmission at the vertical interface.

FDTD animations indicate that for the case of 5 cm, the power circulation between air and slab is reversed with respect to the 1 cm case, i.e., power in the slab travels away from the source, and part of this power leaks to the free-space region, from where it travels backward towards the source. The remaining power in the 5 cm slab gets either transmitted at the second vertical interface (there is a larger field with respect to the 1 cm case on the receive waveguide), attenuated, or weakly contributes to the excitation of polaritons at the trailing edge.

We have also investigated the case of a 1-cm-thick slab with different separations between source and slab, with very

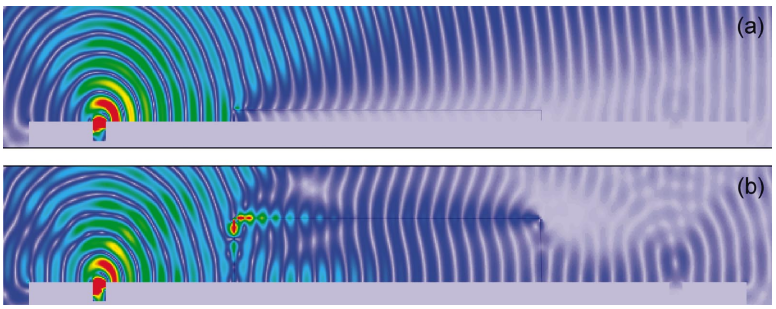

FIG. 5. (Color) FDTD "snapshots" of the electric fields in the time-harmonic regime (after about 50 CW periods). The figure illustrates the effect of LHM slab thickness on the guided wave properties. Cases (a) and (b) correspond to $h=1$ cm and $h=5$ cm, respectively. The corresponding FDTD animations indicate that for case (b), the power circulation between air and slab has been reversed with respect to (a), i.e., power in the slab travels away from the source, and part of this power leaks to the free-space region, from where it travels backward towards the source.

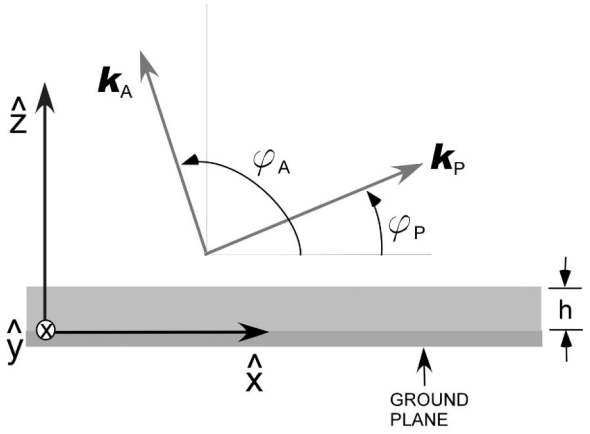

FIG. 6. Definition of propagation angle φ_P and decay angle φ_A.

similar results. The main difference we were able to notice was a very slight enhancement in the power circulation between air and slab, and this occurs only for the case of plane-wave incidence (source of infinite strength at infinity), where the incoming plane wave is grazing at the slab top surface. Because of the similarity, and also for the sake of brevity in the presentation, the corresponding data are not presented here.

B. Theoretical justification: Infinite grounded slab case

In this section, we show that the salient features observed in the FDTD simulations can also be deduced from a time-harmonic analysis of the dominant guided mode within an infinite LHM slab. Specifically, we show that the continuous energy exchange between the slab and free-space region, responsible for sustaining a backward wave within the slab, can be demonstrated in terms of the dominant guided mode. The analysis is carried out in 2D as it includes all the main geometrical features and the salient physics involved. We adopt a field description in terms of guided modes, which is strictly valid only in the neighborhood of the slab. Considering the TM mode with the magnetic field polarized along the y axis (see Fig. 6 for the 2D geometry), a solution to the Maxwell equations yields

$$H = e^{j\omega t}e^{-jk_x x} \times \begin{cases} e^{-\zeta(z-h)}, & z > h \\ \cos(k_z z)/\cos(k_z h), & z < h, \end{cases} \tag{2}$$

where h represents the thickness of the LHM slab, while k_x, k_z, and ζ are spectral coefficients that satisfy

$$k_0^2 = k_x^2 - \zeta^2,$$

$$k^2 = k_x^2 + k_z^2. \tag{3}$$

The coefficients are solutions of transcendental equations given in [18], formed by Eq. (3) and

$$\varepsilon\zeta = \varepsilon_0 k_z \tan(k_z h). \tag{4}$$

By splitting the spectral coefficients into real and imaginary parts as follows:

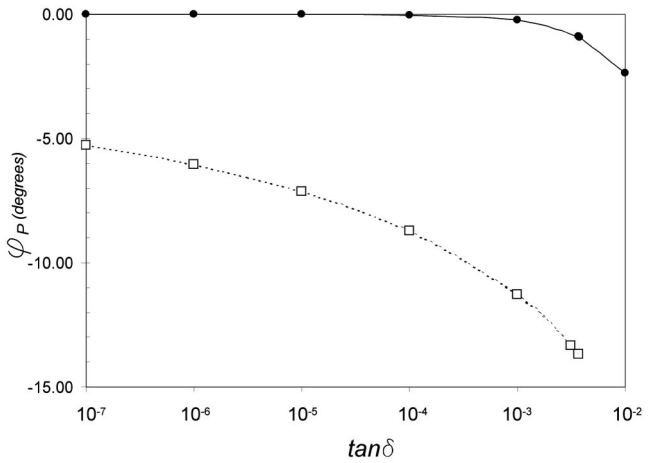

FIG. 7. Propagation angles of leading backward wave modes as a function of loss. The solid and dashed lines denote φ_P for the dominant and next modes, respectively. The LHM slab is 1 cm thick and $f=10$ GHz, $\varepsilon=\mu=-1-j\tan\delta$. The calculation was done using the analysis of [18] adapted to LHM.

$$k_x = \alpha - j\beta,$$

$$k_z = \gamma - j\tau,$$

$$\zeta = \nu - j\rho, \tag{5}$$

it is possible to represent the time-domain fields in the free-space region as

$$\overline{H}(t) = \hat{y}\cos(\omega t - \overline{k_P}\cdot\overline{x})e^{-\overline{k_A}\cdot\overline{x}}, \quad z > h; \tag{6}$$

$$\overline{E}(t) = [\hat{y}\times\overline{k_P}\cos(\omega t - \overline{k_P}\cdot\overline{x}) + \hat{y}\times\overline{k_A}\sin(\omega t - \overline{k_P}\cdot\overline{x})]e^{-\overline{k_A}\cdot\overline{x}}/\omega\varepsilon_0, \quad z > h, \tag{7}$$

where $\overline{k_P}$ and $\overline{k_A}$ are real vectors given by

$$\overline{k_A} = \nu\hat{z} + \beta\hat{x} = |\overline{k_A}|[\cos(\varphi_A)\hat{x} + \sin(\varphi_A)\hat{z}],$$

$$\overline{k_P} = -\rho\hat{z} + \alpha\hat{x} = |\overline{k_P}|[\cos(\varphi_P)\hat{x} + \sin(\varphi_P)\hat{z}]. \tag{8}$$

Equation (8) defines the real angles φ_A and φ_P, which denote the direction of amplitude decay and phase progression, respectively. It is known that in lossless media the direction of propagation is perpendicular to the direction of decay [19]. Figure 6 depicts the directions of propagation and decay, i.e., $\vec{k}_P$ and $\vec{k}_A$, respectively. We expect φ_P and φ_A to be 90° apart.

Following the analysis of [18], we solve the transcendental Eqs. (3) and (4) for a LHM slab, 1 cm thick, characterized by $\varepsilon=\mu=-1-j\tan\delta$, and we examine the resulting propagation angle φ_P at $f=10$ GHz as a function of the loss $\tan\delta$. The dominant backward wave modes as a function of loss are given in Fig. 7. For completeness, we also show the propagation angle associated with the next mode, given by the dashed line. Note that since $\varphi_P<0$, the direction of propagation is towards the slab (at almost grazing angles), indicating that energy is pumped into the slab from the outside. This is in agreement with the earlier FDTD results.

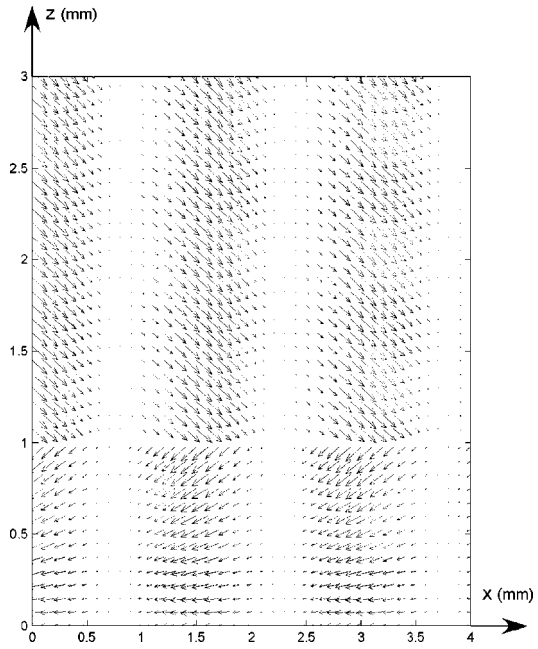

FIG. 8. Map of the Poynting vector fields of the dominant guided mode in the neighborhood of a LHM slab derived from Eq. (9). The fields are mapped for $0 \leqslant x \leqslant 4$ cm, $0 \leqslant z \leqslant 3$ cm, where the LHM slab is the region $0 \leqslant z \leqslant 1$ cm. The results are for $t=0$, $\varepsilon=\mu=-1-j0.013$, $h=1$ cm, $f=10$ GHz, which result in $\varphi_P=-3.081°$ and $|\overline{k_P}|/|\overline{k_A}| \approx 229$. For clarity, the vector component normal to the plane of the slab has been scaled by a factor of 5 so as to be able to observe the power transfer across the interface. The backward wave in the slab is evident from the figure.

We now look at the power flow along the free-space/LHM interface. By means of Eqs. (6) and (7), the time-varying Poynting vector in free space can be written as follows:

$$\overline{P} = \overline{E} \times \overline{H} = \left[\overline{k_P} \cos^2(\omega t - \overline{k_P} \cdot \overline{x}) + \frac{\overline{k_A}}{2} \sin[2(\omega t - \overline{k_P} \cdot \overline{x})] \right] \times e^{-\overline{k_A} \cdot \overline{x}} / \omega \varepsilon_0, \quad z > h. \tag{9}$$

To illustrate the Poynting vector field from Eq. (9), we fix the time and the angle φ_P. As an example for $t=0$, $h=1$ cm, $f=10$ GHz, and $\varepsilon=\mu=-1-j0.03$, the dominant mode is characterized by $\varphi_P=-6.789°$. The corresponding Poynting vector field is presented in Fig. 8, where for convenience the x component of the vector field is again magnified by a factor of 5.[3] The figure is clear evidence that the power within the slab travels towards the source.

Equation (9) indicates that the $\overline{k_A}$ and $\overline{k_P}$ components of the Poynting vector field result in a field map consisting of a succession of "hills and valleys." At the location of the hills, the power travels in the directions dictated by geometrical optics. At the valleys, the situation is more complex, with crossways power components going up on one side of the valley and down on the other side, akin to two antiparallel "fluids." The magnitude of the effect is measured by the relative magnitudes of $|\overline{k_A}|$ and $|\overline{k_P}|$. For the dominant mode, $|\overline{k_P}|/|\overline{k_A}| \approx 229$, i.e., the effect of the double time-harmonic term **(**i.e., $\sin[2(\omega t - \overline{k_P} \cdot \overline{x})]$**)** is negligible. This explains why we do not observe significant power traveling crossways along the valleys in Fig. 8. Importantly, time-harmonic Poynting vector fields obtained from the FDTD simulations for the finite grounded slab in Fig. 4 look very similar to the Poynting vector fields for the infinite one shown in Fig. 8.

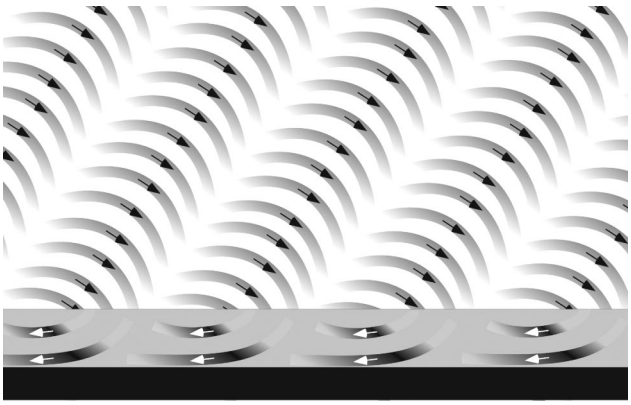

FIG. 9. Sketch of power flow along the free-space/LHM interface provided by Eq. (9). To emphasize the vector fields, we consider here $|\overline{k_A}|$ and $|\overline{k_P}|$ of the same order of magnitude.

To emphasize the overall structure (flow) of these vector fields, we have sketched the general form of the result (9) in Fig. 9, a sketch that considers a scenario where $|\overline{k_A}|$ and $|\overline{k_P}|$ are of the same order of magnitude.

C. Theoretical interpretation

The phenomenon of negative refraction indicates, upon vector decomposition, that the normal components of the Poynting vector are continuous across an air-LHM interface, and that the tangential components of the Poynting vector change sign as we cross the interface. The conducting surface has a strong influence on the guided wave properties of the structure; hence, negative refraction alone does not give an explanation as to why the power in the slab flows towards the source.

Some insight can be gained by considering the case of an electrically thin layer. This is equivalent to a perturbation from the perfectly conducting case, and we can make $k_x=k_0+\xi$ for $\xi \ll k_0$. Using this in Eqs. (3) and (4) results in $\xi \approx (k_0^3 h^2/2\varepsilon^4)(\varepsilon\mu-1)^2$ and $2k_0\xi=\zeta^2$, from which after using $\varepsilon=\mu=-1-j\tan\delta$, we obtain

$$k_x \approx k_0[1-2[k_0 h \tan(\delta)]^2],$$

$$\zeta \approx -2jh\, k_0^2 \tan(\delta). \tag{10}$$

Since $|k_x|<|k_0|$, it follows that propagation in the neighborhood of a thin slab is well represented by a wave impinging on the slab from the free-space region at an angle $\tan^{-1}(\zeta/k_x) \approx -2hk_0\tan(\delta)$, and traveling away from the

[3]For brevity, we have not detailed explicitly the algebraically more complex field expressions for the slab interior, but these have been included in the calculations.

source. In other words, the angle is proportional to the loss tangent of the material (for the case considered in Fig. 8, the approximate angle is −3.12°, which agrees well with the numerical value −3.081° shown in the figure). On the other hand, the time-average power in the x direction inside the slab is given by $\frac{1}{2}\mathrm{Re}\{\hat{x}\cdot(\overline{E}\times\overline{H}^{*})\}$, which can be shown to simplify to $(k_x/2\omega)|\overline{H}|^2\mathrm{Re}(1/\varepsilon)$. Since ε is negative, it is clear that the power inside the slab flows backwards towards the source. Note that this effect could have been explained via negative refraction, provided we had used the knowledge that the wave is essentially grazing the surface. Aside from dissipative losses, such backwards power is provided by the effective wave impinging from the free-space side. It is also clear that in view of Eq. (2), for electrically thin layers, the fields are not concentrated at the air-LHM interface, hence we are not dealing with true polaritons.

As the thickness increases and becomes significant with respect to a wavelength, the solution will incorporate other guided-mode solutions of Eqs. (3) and (4), and eventually, for larger thickness, a combination of higher-order modes resembling Pendry's lens fields will become dominant inside the slab, inverting the state of affairs, i.e., the power inside the slab will be directed away from the source, while the power right above the slab will flow towards the source, as was observed in Fig. 5(b) for the case of a 5 cm slab configuration.

III. CONCLUSIONS

We have demonstrated through FDTD simulations for a grounded LHM plane-parallel finite slab that power recirculation or a feedback loop exists, wherein the fields in the vicinity of the free-space/LHM slab interface exchange power across the interface. For the case of a reasonably thin slab, this sustains a backward wave within the slab; for slabs that exceed a wavelength in thickness, the power loop is inverted, and the scenario is reminiscent of Pendry's ideal lens, with power in the slab traveling away from the source. The transition from thin to thick slab behavior is not abrupt, and is due to the gradual appearance of higher-order modes in the slab. Comparing these results with analytical expressions for an infinite grounded reasonably thin LHM slab confirms that (a) the power in the LHM slab travels towards the source, (b) the dominant mode of operation is an almost grazing backward wave, (c) power in the free-space region provides the energy for the power traveling towards the source in the slab, (d) the fields above and in the neighborhood of the slab are eminently plane wave in nature, impinging towards the slab at an angle proportional to the electrical thickness and the loss tangent of the slab, and (e) the energy accumulates finitely towards the leading edge of the slab. These are all novel effects, not possible with ordinary materials having the potential to be used to generate backward waves in certain devices.

ACKNOWLEDGMENTS

This work was supported in part by the DARPA Metamaterials Program. The authors thank Dr. P.G. Moore, Dr. F.J. Rachford, and Dr. D.L. Smith of NRL for fruitful discussions on diverse LHM issues.

[1] *Radar Cross Section Handbook*, edited by G. T. Ruck (Plenum, New York, 1970).
[2] E. F. Knott, J. F. Shaeffer, and M. T. Tuley, *Radar Cross Section* (Artech House, Boston, 1993).
[3] V. G. Veselago, Sov. Phys. Usp. **10**, 509 (1968).
[4] P. M. Valanju, R. M. Walser, and A. P. Valanju, Phys. Rev. Lett. **88**, 187401 (2002).
[5] J. B. Pendry, Phys. Rev. Lett. **85**, 3966 (2000).
[6] J. B. Pendry and S. A. Ramakrishna, J. Phys.: Condens. Matter **14**, 8463 (2002).
[7] D. R. Smith and N. Kroll, Phys. Rev. Lett. **85**, 2933 (2000).
[8] D. R. Smith, W. J. Padilla, D. C. Vier, S. C. Nemat-Nasser, and S. Schultz, Phys. Rev. Lett. **84**, 4184 (2000).
[9] D. R. Smith, D. C. Vier, N. Kroll, and S. Schultz, Appl. Phys. Lett. **77**, 2246 (2000).
[10] R. A. Shelby, D. R. Smith, S. C. Nemat-Nasser, and S. Schultz, Appl. Phys. Lett. **78**, 489 (2001).
[11] R. A. Shelby, D. R. Smith, and S. Schultz, Science **292**, 77 (2001).
[12] F. J. Rachford, D. L. Smith, P. F. Loschialpo, and D. W. Forester, Phys. Rev. E **66**, 036613 (2002).
[13] J. B. Pendry, A. J. Holden, D. J. Robbins, and W. J. Stewart, IEEE Trans. Microwave Theory Tech. **47**, 2075 (1999).
[14] I. V. Shadrivov, A. A. Sukhorukov, and Y. S. Kivshar, Phys. Rev. E **67**, 057602 (2003).
[15] P. F. Loschialpo, D. W. Forester, D. L. Smith, F. J. Rachford, and C. Monzon, Phys. Rev. E **70**, 036605 (2004).
[16] P. F. Loschialpo, D. L. Smith, D. W. Forester, F. J. Rachford, and J. Schelleng, Phys. Rev. E **67**, 025602 (2003).
[17] J. Berenger, J. Comput. Phys. **114**, 185 (1994).
[18] C. Monzon (unpublished).
[19] R. F. Harrington, *Time Harmonic Electromagnetic Fields* (McGraw-Hill, New York, 1961).